Frontiers of Information Technology & Electronic Engineering
www.jzus.zju.edu.cn; engineering.cae.cn; www.springerlink.com
ISSN 2095-9184 (print); ISSN 2095-9230 (online)
E-mail: jzus@zju.edu.cn

Performance analysis and power allocation of mixed-ADC multi-cell millimeter-wave massive MIMO systems with antenna selection*

Tao ZHOU[1,2], Guichao CHEN[1], Cheng-xiang WANG[3,4], Jiayi ZHANG‡[1], Liu LIU[1], Yiqun LIANG[2]

[1]*School of Electronics and Information Engineering, Beijing Jiaotong University, Beijing 100044, China*

[2]*Center of National Railway Intelligent Transportation System Engineering and Technology, China Academy of Railway Sciences, Beijing 100081, China*

[3]*National Mobile Communications Research Laboratory, School of Information Science and Engineering, Southeast University, Nanjing 210096, China*

[4]*Purple Mountain Laboratories, Nanjing 211111, China*

E-mail: taozhou@bjtu.edu.cn; 17120045@bjtu.edu.cn; chxwang@seu.edu.cn; jiayizhang@bjtu.edu.cn; liuliu@bjtu.edu.cn; liangyiqun@139.com

Received Sept. 28, 2020; Revision accepted Jan. 21, 2021; Crosschecked Feb. 22, 2021

Abstract: In this study, we consider a multi-cell millimeter-wave (mmWave) massive multiple-input multiple-output (MIMO) system with a mixed analog-to-digital converter (mixed-ADC) and hybrid beamforming architecture, in which antenna selection is applied to achieve intelligent assignment of high- and low-resolution ADCs. Both exact and approximate closed-form expressions for the uplink achievable rate are derived in the case of maximum-ratio combining reception. The impacts on the achievable rate of user transmit power, number of radio frequency chains at a base station, ratio of high-resolution ADCs, number of propagation paths, and number of quantization bits are analyzed. It is shown that the user transmit power can be scaled down inversely proportional to the number of antennas at the base station. We propose an efficient power allocation scheme by solving a complementary geometric programming problem. In addition, the energy efficiency is investigated, and an optimal tradeoff between the achievable rate and power consumption is discussed. Our results will provide a useful reference for the study of mixed-ADC multi-cell mmWave massive MIMO systems with antenna selection.

Key words: Millimeter-wave; Massive multiple-input multiple-output (MIMO); Mixed analog-to-digital converter; Performance analysis; Antenna selection
https://doi.org/10.1631/FITEE.2000509 **CLC number:** TN929.5

1 Introduction

Millimeter-wave (mmWave) technology is a disruptive technology to meet the high data rate requirement of fifth generation mobile communication (5G) by providing a large bandwidth. However, the problem of high path loss arises (Boccardi et al., 2014; Wang et al., 2014). Fortunately, the millimeter-scale wavelength allows the transceiver to support a large number of antennas in a small space, and the large antenna arrays can generate high beamforming gains to help mmWave systems overcome high path loss (Yu et al., 2016; Huang et al., 2017; Busari et al.,

‡ Corresponding author

* Project supported by the National Key R&D Program of China (No. 2018YFB1801101), the National Natural Science Foundation of China (Nos. 62071031 and 61960206006), the Beijing Municipal Natural Science Foundation, China (No. 4212006), the Center of National Railway Intelligent Transportation System Engineering and Technology, China Academy of Railway Sciences (Nos. RITS2019KF01 and 2019YJ188), the Research Fund of the National Mobile Communications Research Laboratory, Southeast University, China (Nos. 2020B01 and 2021D01), the Fundamental Research Funds for the Central Universities, China (No. 2242020R30001), the Huawei Cooperation Project, China, and the EU H2020 RISE TESTBED2 Project (No. 872172)

ORCID: Tao ZHOU, https://orcid.org/0000-0001-9908-255X; Jiayi ZHANG, https://orcid.org/0000-0003-2434-4329

2018). The combination of mmWave and massive multiple-input multiple-output (MIMO), through the high beamforming gain, can not only effectively overcome the shortage of high path loss, but also notably improve the system performance by eliminating inter- and intra-cell interference (Huang et al., 2018; Liu et al., 2019; You et al., 2021).

It is well known that the high hardware cost and power consumption limit the deployment of mmWave massive MIMO systems. At present, there are two prospective ways to solve this problem, replacing full-digital architectures with analog-digital hybrid beamforming architectures to decrease the number of radio frequency (RF) chains and substituting high-resolution analog-to-digital converters (ADCs) with low-resolution ADCs to reduce the power consumption and the cost of ADCs (Dai et al., 2020). The coarse quantization of low-resolution ADCs, however, introduces additional overhead for signal processing and front-end design. To alleviate the problem caused by low-resolution ADCs, a mixed-ADC architecture was proposed (Liang and Zhang, 2016), in which only a few high-resolution ADCs were reserved for signal processing and front-end design. Another question is how to determine whether an RF chain is connected to high-resolution ADCs. Until now, in most work on mixed-ADC systems, random connection has been considered (Zhang Y et al., 2020); i.e., the RF chain subsets are randomly selected to connect high-resolution ADCs while the remaining RF chains are connected to low-resolution ADCs. However, the random connection way cannot fully exploit the advantage of high-resolution ADCs, since the channel gain of RF chains connecting high-resolution ADCs can be poor. To make full use of high-resolution ADCs, we employ antenna selection in mixed-ADC systems. We can select an RF chain subset with high channel gain to connect high-resolution ADCs.

1.1 Related works

A few studies have focused on the performance analysis of massive MIMO systems in terms of reducing the quantization resolution of ADCs. For the architecture of low-resolution ADCs, the spectral efficiency (SE) considering maximum-ratio combining (MRC) and zero-forcing (ZF) reception algorithms was investigated using an additive quantization noise model (AQNM) by Orhan et al. (2015) and Qiao et al. (2016), respectively. In particular, on the basis of Bussgang decomposition, Li et al. (2017) studied channel estimation and the achievable rate when only one-bit ADCs were equipped. In Mollén et al. (2017), massive MIMO with orthogonal frequency division multiplexing (OFDM) was considered and the channel capacity of one-bit ADCs was derived. Tan et al. (2016) and Zhang MJ et al. (2018) investigated the SE of mixed-ADC architecture under MRC and ZF reception algorithms, respectively. Zhang JY et al. (2017) found that mixed-ADC architecture would achieve a better tradeoff between SE and energy efficiency (EE) by adjusting the ratio of high-resolution ADCs. Different from studying single-hop systems, a two-hop massive MIMO relaying system with both mixed-ADCs and mixed digital-to-analog converters (mixed-DACs) was investigated (Zhang JY et al., 2019). However, using antenna selection has not been considered in the performance analysis of mixed-ADC massive MIMO systems.

All the above works considered full-digital architectures on low-frequency Rayleigh or Rice fading channels. Little attention has been paid to analog-digital hybrid beamforming architectures over sparse channels for mmWave communications. An analog-digital hybrid beamforming architecture was proposed (Venkateswaran and van der Veen, 2010; Ayach et al., 2012) to reduce power consumption by decreasing the number of RF chains. An overview of sparse channel models and beamforming, precoding, and combining technologies in mmWave band was given by Heath et al. (2016). Choi et al. (2017) proposed a bit-allocation algorithm which adjusts the number of quantization bits of ADCs to maximize SE with the same power consumption. However, only the case in which users configure a single antenna was studied. Achievable rate analysis for multi-cell mmWave massive MIMO systems with low-resolution ADCs was performed by Xu et al. (2019), but they considered only the full-digital architecture.

1.2 Contributions

We concentrate on a multi-cell mmWave massive MIMO system. In contrast to Xu et al. (2019), we consider a hybrid beamforming and mixed-ADC architecture and the employment of antenna selection. Our goal is to analyze the system performance and

investigate the corresponding power allocation scheme. The main contributions are summarized as follows:

1. We derive the exact and approximate closed-form expressions of the uplink achievable rate for a mixed-ADC multi-cell mmWave massive MIMO system with antenna selection. The impacts on the achievable rate of user transmit power, number of RF chains at a base station (BS), ratio of high-resolution ADCs, number of propagation paths, and number of quantization bits are analyzed. The asymptotic analysis shows that the user transmit power can be scaled down inversely proportional to the number of antennas at the BS to maintain a desirable rate.

2. We propose a power allocation scheme to improve the sum achievable rate. The power allocation problem is a general non-convex complementary geometric program (CGP) problem, which can be solved by solving a sequence of geometric program (GP) problems. Compared with uniform allocation, the proposed scheme can significantly increase the sum achievable rate.

3. We study the EE of the system and gain insights into the changes of EE from quantization precision and the ratio of high-resolution ADCs. To maximize EE and achieve the best tradeoff between the achievable rate and power consumption, the optimal number of quantization bits is derived through numerical computation.

Notations used in this paper are as follows: $\boldsymbol{H}^*$, $\boldsymbol{H}^{\mathrm{T}}$, and $\boldsymbol{H}^{\mathrm{H}}$ represent the complex conjugate, transpose, and Hermitian transpose operations of $\boldsymbol{H}$, respectively. $\boldsymbol{h}_i$ is the i^{th} column of $\boldsymbol{H}$. diag($\boldsymbol{H}$) is a diagonal matrix composed of diagonal elements of $\boldsymbol{H}$. $\boldsymbol{I}_N$ represents an N-dimensional identity matrix. $\|\boldsymbol{h}\|$ stands for the 2-norm of vector $\boldsymbol{h}$. $|\cdot|$ is the operation of modulus. $\boldsymbol{H}\in\mathbb{C}^{N\times M}$ indicates that $\boldsymbol{H}$ is an $N\times M$ complex matrix. $\boldsymbol{h}\sim\mathrm{CN}(a, \boldsymbol{B})$ indicates that $\boldsymbol{h}$ is a complex Gaussian vector with mean a and covariance matrix $\boldsymbol{B}$. $\mathbb{E}\{\cdot\}$ denotes the expectation operator.

2 System model

We consider a massive MIMO uplink network with multiple cells, where each cell has one BS with N_{r} antennas serving N_{u} users ($N_{\mathrm{r}}>>N_{\mathrm{u}}$). A user has N_{t} antennas driven by a single RF chain and a BS has N_{RF} RF chains with a mixed-ADC architecture, among which N_{RF0} RF chains are connected to high-resolution ADCs and $N_{\mathrm{RF1}}=N_{\mathrm{RF}}-N_{\mathrm{RF0}}$ RF chains are connected to low-resolution ADCs, as shown in Fig. 1. Unlike previous systems, we add an antenna selection module to select N_{RF0} RF chains with high channel gain at the BS. We define $\gamma \triangleq N_{\mathrm{RF0}}/N_{\mathrm{RF}}\,(0\le\gamma\le 1)$ as the proportion of high-resolution ADCs in the hybrid ADC architecture.

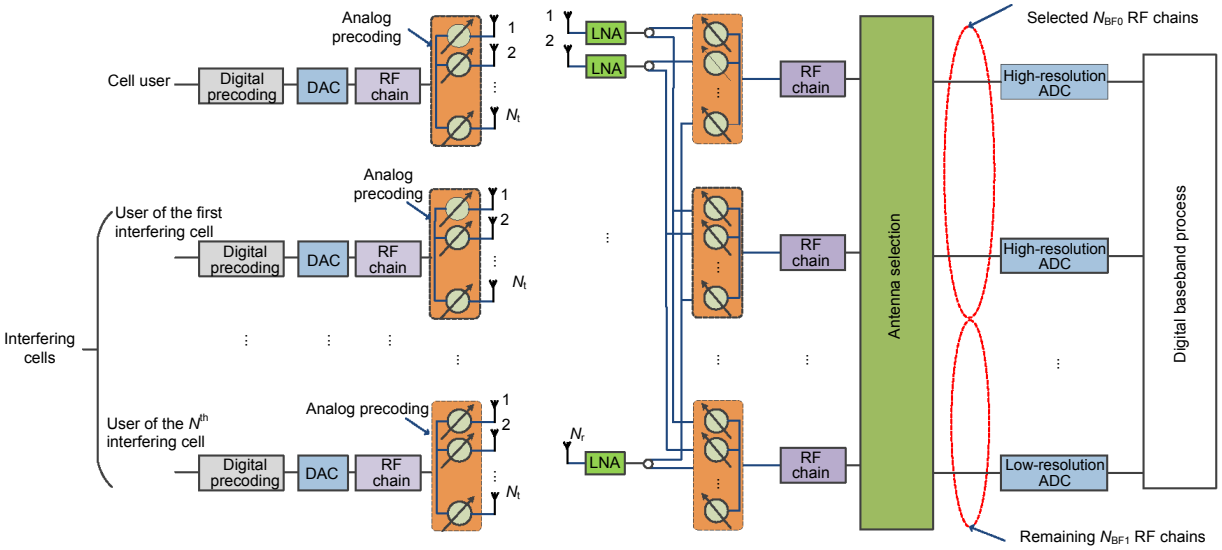

Fig. 1 Hybrid beamforming architecture of the mixed-ADC multi-cell mmWave massive MIMO system with antenna selection

ADC: analog-to-digital converter; DAC: digital-to-analog converter; mmWave: millimeter-wave; MIMO: multiple-input multiple-output; RF: radio frequency; LNA: low noise amplifier

2.1 Signal and channel model

Assume that all N_{u} users of each cell simultaneously transmit mutually independent data symbols to the BS of their respective cells. Due to inter-cell interference, the signal received by the BS is

$$\boldsymbol{y}=\sqrt{\rho}\sum_{k=1}^{N_{\mathrm{u}}}\boldsymbol{p}_k x_k+\sqrt{\rho}\sum_{n=1}^{N}\sum_{k=1}^{N_{\mathrm{u}}}\boldsymbol{p}_{n,k}x_{n,k}+\boldsymbol{z}, \quad (1)$$

where ρ is the user transmit power, N the number of interfering cells, and x_k~CN(0, 1) the signal transmitted by the k^{th} user. $\boldsymbol{p}_k=\boldsymbol{Q}_k\boldsymbol{F}_k\in\mathbb{C}^{N_{\mathrm{r}}\times 1}$ is the channel vector of the k^{th} user. $\boldsymbol{Q}_k\in\mathbb{C}^{N_{\mathrm{r}}\times N_{\mathrm{t}}}$ and $\boldsymbol{F}_k\in\mathbb{C}^{N_{\mathrm{t}}\times 1}$ are the channel matrix and analog precoding vector, respectively. $\boldsymbol{z}\sim\mathrm{CN}(0,\boldsymbol{I}_{N_{\mathrm{r}}})$ is the additive white Gaussian noise (AWGN) vector.

Note that the channel state information (CSI) of each RF chain can be acquired in a round-robin fashion (i.e., only high-resolution ADCs are involved in the channel estimation phase) (Zhang JY et al., 2017). Consequently, the quantization imperfections disappear. Moreover, assume that the channel estimation error is quite small and that the obtained CSI is perfect (Rahimian et al., 2020). Thus, all users' $\boldsymbol{p}_k$ are perfectly known by the BS.

In mmWave band, $\boldsymbol{Q}_k$ can be expressed as

$$\boldsymbol{Q}_k=\sqrt{\beta_k}\sum_{l=1}^{L_k}g_{k,l}\boldsymbol{a}_{\mathrm{r}}(\theta_{k,l})\boldsymbol{a}_{\mathrm{t}}^{\mathrm{H}}(\varphi_{k,l})\in\mathbb{C}^{N_{\mathrm{r}}\times N_{\mathrm{t}}}, \quad (2)$$

where β_k is the large-scale fading gain, L_k~max{Poisson(λ_{p}), 1} (Akdeniz et al., 2014) is the number of propagation paths, and $g_{k,l}$~CN(0, 1) is the small-scale fading gain. Assume that the small-scale fading gain of each propagation path is independent and identically distributed (i.i.d.) (Zhou et al., 2018, 2020a, 2020b). $\boldsymbol{a}_{\mathrm{r}}(\theta_{k,l})\in\mathbb{C}^{N_{\mathrm{r}}\times 1}$ and $\boldsymbol{a}_{\mathrm{t}}(\varphi_{k,l})\in\mathbb{C}^{N_{\mathrm{t}}\times 1}$ are the antenna array responses of the BS and user, respectively.

Assume that the antenna is a uniform linear array (ULA), i.e.,

$$\boldsymbol{a}_{\mathrm{r}}(\theta)=\frac{1}{\sqrt{N_{\mathrm{r}}}}\left[\mathrm{e}^{-\mathrm{j}2\pi\vartheta},\mathrm{e}^{-\mathrm{j}4\pi\vartheta},\cdots,\mathrm{e}^{-\mathrm{j}2\pi(N_{\mathrm{r}}-1)\vartheta}\right]^{\mathrm{T}},$$

$$\boldsymbol{a}_{\mathrm{t}}(\varphi)=\frac{1}{\sqrt{N_{\mathrm{t}}}}\left[\mathrm{e}^{-\mathrm{j}2\pi\phi},\mathrm{e}^{-\mathrm{j}4\pi\phi},\cdots,\mathrm{e}^{-\mathrm{j}2\pi(N_{\mathrm{t}}-1)\phi}\right]^{\mathrm{T}},$$

where $\vartheta=d\sin(\theta)/\lambda$ and $\phi=d\sin(\varphi)/\lambda$ (where d is the spacing between the antennas and λ represents the wavelength).

With Eq. (2), the channel vector $\boldsymbol{p}_k$ in Eq. (1) can be modeled as

$$\boldsymbol{p}_k=\sqrt{\beta_k}\sum\nolimits_{l=1}^{L_k}g_{k,l}c_{k,l}\boldsymbol{a}_{\mathrm{r}}(\theta_{k,l}), \quad (3)$$

where $c_{k,l}=\boldsymbol{a}_{\mathrm{r}}^{\mathrm{H}}(\varphi_{k,l})\boldsymbol{F}_k$ is the beamforming gain.

Consider that θ refers to the uniformly spaced spatial angle, i.e., $\vartheta_i=d\sin(\theta_i)/\lambda=(i-1)/N_{\mathrm{r}}$, $i=1, 2, \ldots, N_{\mathrm{r}}$. Matrix $\boldsymbol{E}=\left[\boldsymbol{a}_{\mathrm{r}}(\theta_1),\boldsymbol{a}_{\mathrm{r}}(\theta_2),\ldots,\boldsymbol{a}_{\mathrm{r}}(\theta_{N_{\mathrm{r}}})\right]$ defined by θ is a unitary DFT matrix, $\boldsymbol{E}\boldsymbol{E}^{\mathrm{H}}=\boldsymbol{E}^{\mathrm{H}}\boldsymbol{E}=\boldsymbol{I}$. Channel vector $\boldsymbol{p}_k$ in Eq. (3) can be modeled as

$$\boldsymbol{p}_k=\sum\nolimits_{i=1}^{N_{\mathrm{r}}}h_{k,i}\boldsymbol{a}_{\mathrm{r}}(\theta_i)=\boldsymbol{E}\tilde{\boldsymbol{h}}_k, \quad (4)$$

where $\tilde{\boldsymbol{h}}_k\in\mathbb{C}^{N_{\mathrm{r}}\times 1}$ is the beamspace channel vector with non-zero elements. Each non-zero element L_k consists of a large-scale fading gain β_k, a small-scale fading gain $g_{k,l}$, and a beamforming gain $c_{k,l}$.

So, the signal received by the BS in Eq. (1) can be expressed as

$$\boldsymbol{y}=\sqrt{\rho}\tilde{\boldsymbol{H}}\boldsymbol{x}+\sqrt{\rho}\sum\nolimits_{n=1}^{N}\tilde{\boldsymbol{H}}_n\boldsymbol{x}_n+\boldsymbol{z}, \quad (5)$$

where $\tilde{\boldsymbol{H}}=\boldsymbol{E}\left[\tilde{\boldsymbol{h}}_1,\tilde{\boldsymbol{h}}_2,\ldots,\tilde{\boldsymbol{h}}_{N_{\mathrm{u}}}\right]\in\mathbb{C}^{N_{\mathrm{r}}\times N_{\mathrm{u}}}$ and $\boldsymbol{x}\in\mathbb{C}^{N_{\mathrm{u}}\times 1}$ are the channel and signal of all users in a cell, respectively.

Assume that the analog receive beamforming matrix in Fig. 1 is a sub-matrix of $\boldsymbol{E}$, i.e., $\boldsymbol{W}_{\mathrm{RF}}=\boldsymbol{E}_{\mathrm{RF}}\in\mathbb{C}^{N_{\mathrm{r}}\times N_{\mathrm{RF}}}$, and further assume that $\boldsymbol{E}_{\mathrm{RF}}$ contains all the user transmission paths (Heath et al., 2016). Then the signal processed by the receive beamforming matrix is

$$\begin{aligned}\tilde{\boldsymbol{y}}&=\sqrt{\rho}\boldsymbol{W}_{\mathrm{RF}}^{\mathrm{H}}\tilde{\boldsymbol{H}}\boldsymbol{x}+\sqrt{\rho}\sum_{n=1}^{N}\boldsymbol{W}_{\mathrm{RF}}^{\mathrm{H}}\tilde{\boldsymbol{H}}_n\boldsymbol{x}_n+\boldsymbol{W}_{\mathrm{RF}}^{\mathrm{H}}\boldsymbol{z}\\&=\sqrt{\rho}\boldsymbol{H}\boldsymbol{x}+\sqrt{\rho}\sum_{n=1}^{N}\boldsymbol{H}_n\boldsymbol{x}_n+\boldsymbol{n},\end{aligned} \quad (6)$$

where $\boldsymbol{H}=\left[\boldsymbol{h}_1,\boldsymbol{h}_2,\cdots,\boldsymbol{h}_{N_\mathrm{u}}\right]\in\mathbb{C}^{N_\mathrm{RF}\times N_\mathrm{u}}$ is a sub-matrix of $\left[\tilde{\boldsymbol{h}}_1,\tilde{\boldsymbol{h}}_2,\ldots,\tilde{\boldsymbol{h}}_{N_\mathrm{u}}\right]$ and contains all the user transmission paths. $\boldsymbol{n}=\boldsymbol{W}_\mathrm{RF}^\mathrm{H}\boldsymbol{z}\sim\mathrm{CN}(0,\boldsymbol{I}_{N_\mathrm{r}})$, because $\boldsymbol{W}_\mathrm{RF}$ is a unitary matrix.

Compared to the random connection method, we employ antenna selection to decide whether to connect an RF chain to high-resolution ADCs. We first use antenna selection algorithms to select N_RF0 RF chains with high channel gain, and then connect the selected N_RF0 RF chains to high-resolution ADCs and the remaining N_RF1 RF chains to low-resolution ADCs.

Define $\boldsymbol{H}_0\in\mathbb{C}^{N_\mathrm{RF0}\times N_\mathrm{u}}$ as the channel between all users with N_RF0 RF chains selected by the antenna selection algorithms and $\boldsymbol{H}_1\in\mathbb{C}^{N_\mathrm{RF1}\times N_\mathrm{u}}$ as the channel between all users with the remaining N_RF1 RF chains. Therefore, the received signal in Eq. (6) can be expressed as

$$\tilde{\boldsymbol{y}}=\begin{bmatrix}\tilde{\boldsymbol{y}}_0\\ \tilde{\boldsymbol{y}}_1\end{bmatrix}=\begin{bmatrix}\sqrt{\rho}\boldsymbol{H}_0\boldsymbol{x}+\sqrt{\rho}\sum_{n=1}^{N}\boldsymbol{H}_{n,0}\boldsymbol{x}_n+\boldsymbol{n}_0\\ \sqrt{\rho}\boldsymbol{H}_1\boldsymbol{x}+\sqrt{\rho}\sum_{n=1}^{N}\boldsymbol{H}_{n,1}\boldsymbol{x}_n+\boldsymbol{n}_1\end{bmatrix}. \quad (7)$$

2.2 Quantization model for mixed-resolution ADCs

Consider that all low-resolution ADCs have the same number of quantization bits and adopt AQNM to transform the nonlinear quantization process into a linear form. The signal after quantization is

$$\begin{aligned}\boldsymbol{y}_\mathrm{q}&=\begin{bmatrix}\tilde{\boldsymbol{y}}_0\\ Q(\tilde{\boldsymbol{y}}_1)\end{bmatrix}\\&=\begin{bmatrix}\sqrt{\rho}\boldsymbol{H}_0\boldsymbol{x}+\sqrt{\rho}\sum_{n=1}^{N}\boldsymbol{H}_{n,0}\boldsymbol{x}_n+\boldsymbol{n}_0\\ \alpha\sqrt{\rho}\boldsymbol{H}_1\boldsymbol{x}+\sqrt{\rho}\sum_{n=1}^{N}\boldsymbol{H}_{n,1}\boldsymbol{x}_n+\alpha\boldsymbol{n}_1+\boldsymbol{n}_\mathrm{q}\end{bmatrix},\end{aligned} \quad (8)$$

where $Q(\cdot)$ is the quantization function, $\alpha=1-\delta$ is the quantization gain, and δ is the distortion factor determined by the number of quantization bits b. The exact values of δ are listed in Table 1 when $b\leq5$, and $\delta\approx\sqrt{3}\pi2^{-2b}/2$ when $b>5$ (Zhang JY et al., 2019). $\boldsymbol{n}_\mathrm{q}$ is the additive quantization noise, and the covariance matrix of $\boldsymbol{n}_\mathrm{q}$ is

$$\boldsymbol{R}_{\boldsymbol{n}_\mathrm{q}}=\alpha(1-\alpha)\mathrm{diag}\left(\rho\bar{\boldsymbol{H}}_1\boldsymbol{R}_{\boldsymbol{x}}\bar{\boldsymbol{H}}_1^\mathrm{H}+\boldsymbol{I}_{N_\mathrm{RF1}}\right), \quad (9)$$

where $\bar{\boldsymbol{H}}_1=\left[\boldsymbol{H}_1,\boldsymbol{H}_{1,1},\boldsymbol{H}_{2,1},\ldots,\boldsymbol{H}_{N,1}\right]\in\mathbb{C}^{N_\mathrm{RF1}\times(N+1)N_\mathrm{u}}$ is the channel between all users with N_RF1 RF chains connected to low-resolution ADCs, and $\boldsymbol{R}_{\boldsymbol{x}}$ is the covariance matrix of the transmitted signal. In this study, we assume $\boldsymbol{x}\sim\mathrm{CN}(0,1)$. So, $\boldsymbol{R}_{\boldsymbol{x}}=\boldsymbol{I}$. Eq. (9) can be expressed as

$$\boldsymbol{R}_{\boldsymbol{n}_\mathrm{q}}=\alpha(1-\alpha)\mathrm{diag}\left(\rho\bar{\boldsymbol{H}}_1\bar{\boldsymbol{H}}_1^\mathrm{H}+\boldsymbol{I}_{N_\mathrm{RF1}}\right). \quad (10)$$

Table 1 Values of δ for different values of b

b	δ	b	δ
1	0.3634	4	0.0095
2	0.1175	5	0.0025
3	0.0345		

3 Uplink achievable rate

In this section, we first derive the closed-form expression of the uplink achievable rate for the MRC receive algorithm, and then show that the performance loss caused by low-resolution ADCs can be compensated for by increasing the number of RF chains.

3.1 Exact achievable rate

Let $\boldsymbol{A}$ be an $N_\mathrm{RF}\times N_\mathrm{u}$ digital receive matrix in Fig. 1. Similar to $\boldsymbol{H}$, we decompose $\boldsymbol{A}$ into $\boldsymbol{A}_0\in\mathbb{C}^{N_\mathrm{RF0}\times N_\mathrm{u}}$ and $\boldsymbol{A}_1\in\mathbb{C}^{N_\mathrm{RF1}\times N_\mathrm{u}}$:

$$\boldsymbol{A}=\begin{bmatrix}\boldsymbol{A}_0\\ \boldsymbol{A}_1\end{bmatrix}. \quad (11)$$

The quantized signal vector in Eq. (8) is processed as

$$\begin{aligned}\boldsymbol{r}=\boldsymbol{A}^\mathrm{H}\boldsymbol{y}_\mathrm{q}&=\sqrt{\rho}\boldsymbol{A}_0^\mathrm{H}\boldsymbol{H}_0\boldsymbol{x}+\sqrt{\rho}\sum\nolimits_{n=1}^{N}\boldsymbol{A}_0^\mathrm{H}\boldsymbol{H}_{n,0}\boldsymbol{x}_n\\&+\boldsymbol{A}_0^\mathrm{H}\boldsymbol{n}_0+\alpha\sqrt{\rho}\boldsymbol{A}_1^\mathrm{H}\boldsymbol{H}_1\boldsymbol{x}+\alpha\sqrt{\rho}\sum\nolimits_{n=1}^{N}\boldsymbol{A}_1^\mathrm{H}\boldsymbol{H}_{n,1}\boldsymbol{x}_n\\&+\alpha\boldsymbol{A}_1^\mathrm{H}\boldsymbol{n}_1+\boldsymbol{A}_1^\mathrm{H}\boldsymbol{n}_\mathrm{q}.\end{aligned} \quad (12)$$

The received signal of the k^{th} user can be expressed as

$$\begin{aligned}\boldsymbol{r}_k=&\sqrt{\rho}\boldsymbol{a}_{k,0}^{\mathrm{H}}\boldsymbol{h}_{k,0}x_k+\alpha\sqrt{\rho}\boldsymbol{a}_{k,1}^{\mathrm{H}}\boldsymbol{h}_{k,1}x_k+\sqrt{\rho}\sum_{j=1,j\neq k}^{N_{\mathrm{u}}}\boldsymbol{a}_{k,0}^{\mathrm{H}}\boldsymbol{h}_{j,0}x_j\\&+\sqrt{\rho}\sum_{n=1}^{N}\sum_{j=1}^{N_{\mathrm{u}}}\boldsymbol{a}_{k,0}^{\mathrm{H}}\boldsymbol{h}_{n,j,0}x_{n,j}+\alpha\sqrt{\rho}\sum_{j=1,j\neq k}^{N_{\mathrm{u}}}\boldsymbol{a}_{k,1}^{\mathrm{H}}\boldsymbol{h}_{j,1}x_j\\&+\alpha\sqrt{\rho}\sum_{n=1}^{N}\sum_{j=1}^{N_{\mathrm{u}}}\boldsymbol{a}_{k,1}^{\mathrm{H}}\boldsymbol{h}_{n,j,1}x_{n,j}+\boldsymbol{a}_{k,0}^{\mathrm{H}}\boldsymbol{n}_0+\alpha\boldsymbol{a}_{k,1}^{\mathrm{H}}\boldsymbol{n}+\boldsymbol{a}_{k,1}^{\mathrm{H}}\boldsymbol{n}_{\mathrm{q}},\end{aligned}\tag{13}$$

where $\boldsymbol{a}_{k,0}$ is the k^{th} column of $\boldsymbol{A}_0$ and $\boldsymbol{a}_{k,1}$ is the k^{th} column of $\boldsymbol{A}_1$. The achievable rate of the k^{th} user is

$$R_k=\mathbb{E}\left\{\log_2\left(1+\frac{D_k}{J_k}\right)\right\},\tag{14}$$

where

$$D_k=\rho\left(\left|\boldsymbol{a}_{k,0}^{\mathrm{H}}\boldsymbol{h}_{k,0}\right|^2+\alpha^2\left|\boldsymbol{a}_{k,1}^{\mathrm{H}}\boldsymbol{h}_{k,1}\right|^2+2\alpha\boldsymbol{a}_{k,0}^{\mathrm{H}}\boldsymbol{h}_{k,0}\boldsymbol{h}_{k,1}^{\mathrm{H}}\boldsymbol{a}_{k,1}\right)\tag{15}$$

is the desired signal power and

$$\begin{aligned}J_k=&\rho\sum_{j=1,j\neq k}^{N_{\mathrm{u}}}\left|\boldsymbol{a}_{k,0}^{\mathrm{H}}\boldsymbol{h}_{j,0}\right|^2+\alpha^2\rho\sum_{j=1,j\neq k}^{N_{\mathrm{u}}}\left|\boldsymbol{a}_{k,1}^{\mathrm{H}}\boldsymbol{h}_{j,1}\right|^2\\&+\rho\sum_{n=1}^{N}\sum_{j=1}^{N_{\mathrm{u}}}\left|\boldsymbol{a}_{k,0}^{\mathrm{H}}\boldsymbol{h}_{n,j,0}\right|^2+\alpha^2\rho\sum_{n=1}^{N}\sum_{j=1}^{N_{\mathrm{u}}}\left|\boldsymbol{a}_{k,1}^{\mathrm{H}}\boldsymbol{h}_{n,j,1}\right|^2\\&+\left\|\boldsymbol{a}_{k,0}\right\|^2+\alpha^2\left\|\boldsymbol{a}_{k,1}\right\|^2+\boldsymbol{a}_{k,1}^{\mathrm{H}}\boldsymbol{R}_{\boldsymbol{n}_{\mathrm{q}}}\boldsymbol{a}_{k,1}\end{aligned}\tag{16}$$

is the interference-plus-noise power.

Then we will derive the closed-form expression of the uplink achievable rate for the k^{th} user in Eq. (13).

Theorem 1 For mixed-ADC multi-cell mmWave massive MIMO systems and using the MRC receive algorithms with prefect CSI at the BS, the closed-form expression of the k^{th} user achievable rate is given as

$$R_k=\log_2\left(1+\frac{M_k}{N_k+O_k+P_k+S_k}\right),\tag{17}$$

where

$$\begin{aligned}M_k=&\rho\beta_k\left(\lambda_{\mathrm{p}}+\mathrm{e}^{-\lambda_{\mathrm{p}}}\right)\left[\overline{\left|c_{k,0}\right|^4}\gamma+\alpha^2\overline{\left|c_{k,1}\right|^4}(1-\gamma)\right]\\&+2\alpha\rho\beta_k\left(\lambda_{\mathrm{p}}^2+\lambda_{\mathrm{p}}+\mathrm{e}^{-\lambda_{\mathrm{p}}}\right)\overline{\left|c_{k,0}\right|^2\left|c_{k,1}\right|^2}\gamma(1-\gamma)\\&+\rho\beta_k\left(\lambda_{\mathrm{p}}^2+\lambda_{\mathrm{p}}+e^{-\lambda_{\mathrm{p}}}\right)\\&\cdot\left[\left(\overline{\left|c_{k,0}\right|^2}\right)^2\gamma^2+\alpha^2\left(\overline{\left|c_{k,1}\right|^2}\right)^2(1-\gamma)^2\right],\end{aligned}\tag{18}$$

$$\begin{aligned}N_k=&\rho\left(\lambda_{\mathrm{p}}+\mathrm{e}^{-\lambda_{\mathrm{p}}}\right)^2\\&\cdot\sum_{j=1,j\neq k}^{N_{\mathrm{u}}}\beta_j\frac{\overline{\left|c_{k,0}\right|^2\left|c_{j,0}\right|^2}\gamma+\alpha\overline{\left|c_{k,1}\right|^2\left|c_{j,1}\right|^2}(1-\gamma)}{N_{\mathrm{RF}}},\end{aligned}\tag{19}$$

$$\begin{aligned}O_k=&\rho\left(\lambda_{\mathrm{p}}+\mathrm{e}^{-\lambda_{\mathrm{p}}}\right)^2\\&\cdot\sum_{n=1}^{N}\sum_{j=1}^{N_{\mathrm{u}}}\beta_{n,j}\frac{\overline{\left|c_{k,0}\right|^2\left|c_{n,j,0}\right|^2}\gamma+\alpha\overline{\left|c_{k,1}\right|^2\left|c_{n,j,1}\right|^2}(1-\gamma)}{N_{\mathrm{RF}}},\end{aligned}\tag{20}$$

$$P_k=\left(\lambda_{\mathrm{p}}+\mathrm{e}^{-\lambda_{\mathrm{p}}}\right)\left[\overline{\left|c_{k,0}\right|^2}\gamma+\alpha\overline{\left|c_{k,1}\right|^2}(1-\gamma)\right],\tag{21}$$

$$S_k=2\alpha(1-\alpha)\rho\beta_k\left(\lambda_{\mathrm{p}}+\mathrm{e}^{-\lambda_{\mathrm{p}}}\right)\overline{\left|c_{k,1}\right|^4}(1-\gamma),\tag{22}$$

where $\overline{\left|c_{k,0}\right|^i}=\sum_{l=1}^{L_0}\left|c_{k,l}\right|^i/L_0$ and $\overline{\left|c_{k,1}\right|^i}=\sum_{l=L_0+1}^{L}\left|c_{k,l}\right|^i/L_1$ are the mean values of $\left|c_{k,0}\right|^i$ and $\left|c_{k,1}\right|^i$, respectively (L_0 is the number of propagation paths in RF chains connected to high-resolution ADCs, L_1 is the number of propagation paths in RF chains connected to low-resolution ADCs, and i is 2 or 4).

Proof is provided in the Appendix.

3.2 Asymptotic achievable rate analysis

From Theorem 1, we can obtain that the achievable rate of the k^{th} user is related to the transmit power ρ, number of propagation paths λ_{p}, beamforming gain $c_{k,l}$, number of RF chains N_{RF}, and number of ADC quantization bits b. To have a profound understanding of Theorem 1, we use Corollary 1 and provide a few remarks on the achievable rate as follows:

Corollary 1 When the number of propagation paths λ_{p} is large and users have only a single antenna,

Eq. (17) can be approximated as

$$\tilde{R}_k \approx \log_2\left(1+\frac{T_k}{I_{k,1}+I_{k,2}+I_{k,3}}\right), \tag{23}$$

where

$$T_k=\rho\beta_k\left\{[\gamma+\alpha^2(1-\gamma)]+(\lambda_\mathrm{p}+1)[\gamma+\alpha(1-\gamma)]^2\right\}, \tag{24}$$

$$I_{k,1}=\rho\lambda_\mathrm{p}\frac{\gamma+\alpha(1-\gamma)}{N_\mathrm{RF}}\left(\sum_{j=1,j\neq k}^{N_\mathrm{u}}\beta_j+\sum_{n=1}^{N}\sum_{j=1}^{N_\mathrm{u}}\beta_{n,j}\right), \tag{25}$$

$$I_{k,2}=\gamma+\alpha(1-\gamma), \tag{26}$$

$$I_{k,3}=2\alpha(1-\alpha)\rho\beta_k(1-\gamma). \tag{27}$$

Proof When λ_p is large, $\lambda_\mathrm{p}+\mathrm{e}^{-\lambda_\mathrm{p}}\approx\lambda_\mathrm{p}$. When users have only a single antenna, $c_{k,l}$=1. Substituting $\lambda_\mathrm{p}+\mathrm{e}^{-\lambda_\mathrm{p}}\approx\lambda_\mathrm{p}$ and $c_{k,l}$=1 into Eq. (17), we can obtain the result.

In Eq. (23), we can find that the performance loss caused by low-resolution ADCs can be compensated for by increasing the transmit power of users and the number of RF chains.

Remark 1 With fixed N_BF and b, when $\rho\to\infty$, Eq. (23) increases to

$$\tilde{R}_k\to\log_2\left(1+\frac{T_k}{I_{k,1}+I_{k,3}}\right). \tag{28}$$

It is clear in Eq. (28) that using more RF chains can improve the achievable rate by reducing inter- and intra-cell interference. When $N_\mathrm{RF}\to\infty$, Eq. (28) increases to

$$\tilde{R}_k\to\log_2\left(1+\frac{\gamma+\alpha^2(1-\gamma)}{2\alpha(1-\alpha)(1-\gamma)}+\frac{(\lambda_\mathrm{p}+1)\left[\gamma+\alpha(1-\gamma)\right]^2}{2\alpha(1-\alpha)(1-\gamma)}\right). \tag{29}$$

Eq. (29) shows that increasing the transmit power and the number of RF chains to infinity will make the rate approach a constant related to the number of quantization bits. This indicates that the performance degradation by low-resolution ADCs to the achievable rate cannot be eliminated by increasing the user transmit power and the number of RF chains.

Remark 2 With fixed N_BF and ρ, when $b\to\infty$, Eq. (23) converges to

$$\tilde{R}_k\to\log_2\left(1+\frac{\rho\beta_k(\lambda_\mathrm{p}+2)}{\rho\lambda_\mathrm{p}\dfrac{1}{N_\mathrm{RF}}\left(\displaystyle\sum_{j=1,j\neq k}^{N_\mathrm{u}}\beta_j+\sum_{n=1}^{N}\sum_{j=1}^{N_\mathrm{u}}\beta_{n,j}\right)+1}\right). \tag{30}$$

Similar to Eq. (28), we can increase the number of RF chains to improve the achievable rate by reducing inter- and intra-cell interference. When $N_\mathrm{RF}\to\infty$, the full-resolution achievable rate in Eq. (30) increases to

$$\tilde{R}_k\to\log_2\left[1+\rho\beta_k(\lambda_\mathrm{p}+2)\right]. \tag{31}$$

Eq. (31) shows that even an infinite number of antennas cannot make the full-resolution achievable rate increase to infinity with fixed λ_p. The reason is that increasing the number of antennas does not eliminate the interference of AWGN on the signal.

Remark 3 With fixed b and ρ, without loss of generality, assume that $N_\mathrm{RF}=\mu N_\mathrm{r}$ and $\lambda_\mathrm{p}=\nu N_\mathrm{r}$, where $0<\mu$, $\nu<1$. Eq. (23) reduces to

$$\hat{R}_k\approx\log_2\left(1+\frac{U_k}{I_{k,4}+I_{k,5}}\right), \tag{32}$$

where

$$U_k=\rho\beta_k\left\{[\gamma+\alpha^2(1-\gamma)]+(\nu N_\mathrm{r}+1)[\gamma+\alpha(1-\gamma)]^2\right\}, \tag{33}$$

$$I_{k,4}=\rho[\gamma+\alpha(1-\gamma)]\frac{\nu}{\mu}\left(\sum_{j=1,j\neq k}^{N_\mathrm{u}}\beta_j+\sum_{n=1}^{N}\sum_{j=1}^{N_\mathrm{u}}\beta_{n,j}\right), \tag{34}$$

$$I_{k,5}=[\gamma+\alpha(1-\gamma)]+2\alpha(1-\alpha)\rho\beta_k(1-\gamma). \tag{35}$$

Different from Eqs. (29) and (31), the achievable rate in Eq. (32) will increase indefinitely with the increase in the antenna number. This is because the number of propagation paths λ_p is not fixed as in Remarks 1 and 2.

Remark 4 On the basis of Remark 3, we further assume that the transmit power is inversely proportional to the number of RF chains, i.e., $\rho=E_\mathrm{u}/N_\mathrm{RF}$.

When $N_r \to \infty$, Eq. (32) reduces to

$$\hat{R}_k \to \log_2\left(1+\frac{E_u\beta_k v[\gamma+\alpha(1-\gamma)]}{\mu}\right), \quad (36)$$

where E_u is a constant. Eq. (36) shows that we can scale down the average transmit power ρ proportional to $1/N_r$ and maintain the same achievable rate. Meanwhile, the result is consistent with that in Remark 5 in Choi et al. (2017) when γ=0.

4 Power allocation

As seen in Remark 1, we cannot enhance the achievable rate by simply increasing the transmit power. This is because boosting the transmit power will enhance both the desired and interfering signals. In this section, we study the optimal power allocation to maximize the sum rate of the mixed-ADC multi-cell mmWave massive MIMO system with a total power P_T.

This optimization problem can be expressed as

$$P_1: \max_{\boldsymbol{\rho}, P_B} \sum_{k=1}^{N_u} R_k \text{ subject to} \sum_{k=1}^{N_u} \rho_k + P_B \le P_T, \quad \boldsymbol{\rho} \ge 0,\ P_B \ge 0, \quad (37)$$

where $\boldsymbol{\rho}=[\rho_1,\rho_2,...,\rho_{N_u}]^T$ is a transmit power vector, and P_B is the power consumed by the BS which determines the ratio of high-resolution ADCs and the number of quantization bits.

According to Eq. (17), P_1 can be reformulated as

$$P_2: \min_{\boldsymbol{\rho}, P_B} \prod_{k=1}^{N_u}(1+\xi_k)^{-1} \text{ subject to } \sum_{k=1}^{N_u}\rho_k + P_B \le P_T, \quad \boldsymbol{\rho} \ge 0,\ P_B \ge 0, \quad (38)$$

where $\xi_k=M_k/(N_k+O_k+P_k+S_k)$ is the signal-to-interference-plus-noise ratio (SINR) of the k^{th} user. P_2 is a general non-convex CGP optimization problem. At present, we can obtain only its approximate solution by solving a sequence of GP problems. As for the GP problems, we use standard convex optimization tools to solve them. Algorithm 1 describes the specific steps to settle problem P_2.

Algorithm 1 Successive approximation algorithm for P_2

(1) Initialization: Define tolerance ε and parameter ω. Set j=1 and the initial value $\overline{\xi_k}$ according to SINR in Theorem 1, with $\rho_k=P_T/(2N_u)$ and $P_B=P_T/2$.

(2) Iteration j: Compute $v_k=\overline{\xi_k}/(1+\xi_k)$. Then solve the GP problem P_3:

$$P_3: \min_{\boldsymbol{\rho}, P_B} \prod_{k=1}^{N_u}\xi_k^{-v_k} \text{ subject to } \omega^{-1}\tilde{\xi}_k \le \xi_k \le \omega\tilde{\xi}_k,$$
$$\xi_k\rho_k^{-1}\xi_k \le 1,\ k=1,2,...,N_u, \quad (39)$$
$$\sum_{k=1}^{N_u}\rho_k + P_B \le P_T,\ \boldsymbol{\rho} \ge 0,\ P_B \ge 0.$$

Denote the optimal solution by $\xi_k^{(j)}$ for k=1, 2, …, N_u.

(3) Stopping criterion: If $\max_k\left|\xi_k^{(j)}-\overline{\xi_k}\right|<\varepsilon$, then stop; otherwise, go to step (4).

(4) Updating the initial values: Set $\overline{\xi_k}=\xi_k^{(j)}$ and j=j+1. Go to step (2).

5 Results and discussion

Simulation results are given in this section to verify the correctness of the closed-form expression in Eq. (17) and analyze the benefits to the system performance of using antenna selection algorithms. Then, the benefit of the power allocation algorithm is illustrated. In addition, we explore EE to show that the mixed-ADC architecture can achieve a better tradeoff between SE and EE.

Unless otherwise specified, the following simulation parameters are assumed: The number of interfering cells is 6, and each cell has eight users who are randomly distributed at a distance of 30 to 200 m from the BS, i.e., $30 \le d \le 200$, where d is the distance between the user and BS. The large-scale fading gain β=72+29.2log$d$+ψ (dB) (Abbas et al., 2017), where ψ~CN(0, 8.7) is the shadow fading gain. Assume that the number of RF chains $N_{RF}=0.5N_r$ and the number of propagation paths $\lambda_p=0.1N_r$.

5.1 Achievable rate

To explore the performance improvement of applying antenna selection algorithms in mixed-resolution ADC systems, the sum rate of a multi-cell

mmWave massive MIMO system with the cases of antenna selection and random connection is depicted in Figs. 2–7. Note that antenna selection means that we select N_{RF0} antennas according to the antenna selection algorithm proposed in Choi et al. (2018) to connect high-resolution ADCs, whereas random connection means that the random antenna selection mode is employed.

Fig. 2 illustrates the simulation results in Eq. (14) and closed-form expression results in Eq. (17) over the number of antennas with high-resolution ADC ratio γ=0.1 and the number of quantization bits b=1, 2, ∞. We can see that the results in simulation and Theorem 1 are approximately equal and that the trend is consistent. This proves the correctness of the results we have obtained in Eq. (17).

Fig. 3 shows the sum rate over the transmit power ρ with high-resolution ADC ratio γ=0.5 and the number of BS antennas N_r=256 for the number of quantization bits b=1, 2. We can see in Fig. 3 that applying the antenna selection algorithm significantly increases the sum rate in the considered system at any signal-to-noise ratio (SNR). When b=1, the system performance using the antenna selection algorithm increases by about 20%, while the improvement is only 5% when b=2. Therefore, the antenna selection algorithm improves the system performance more significantly when b is small. It can also be seen that the sum rate does not increase with transmit power to infinity but reaches a constant. This proves the correctness of Remark 1.

In Fig. 4, we investigate the uplink sum achievable rate over the number of antennas with the number of quantization bits b=1 for high-resolution ADC ratio γ=0.1, 0.5. Figs. 4a and 4b show fixed transmit power ρ=30 dB and the power scaling law of

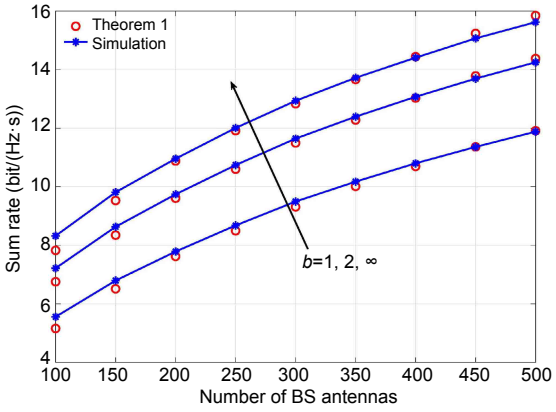

Fig. 2 Uplink sum rate derived from the simulation and Theorem 1 against the number of antennas N_r for ρ=30 dB, γ=0.1, and b=1, 2, ∞

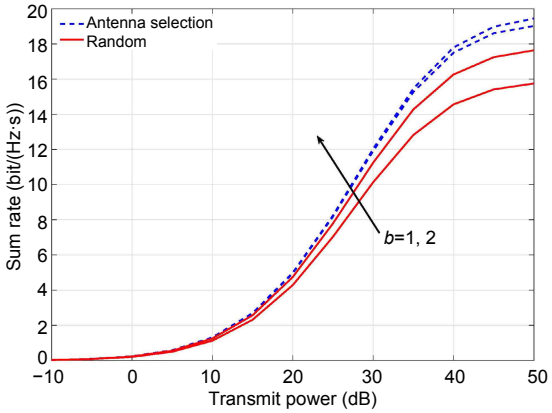

Fig. 3 Uplink sum rate of antenna selection and random connection against the transmit power ρ for N_r=256, γ=0.5, and b=1, 2

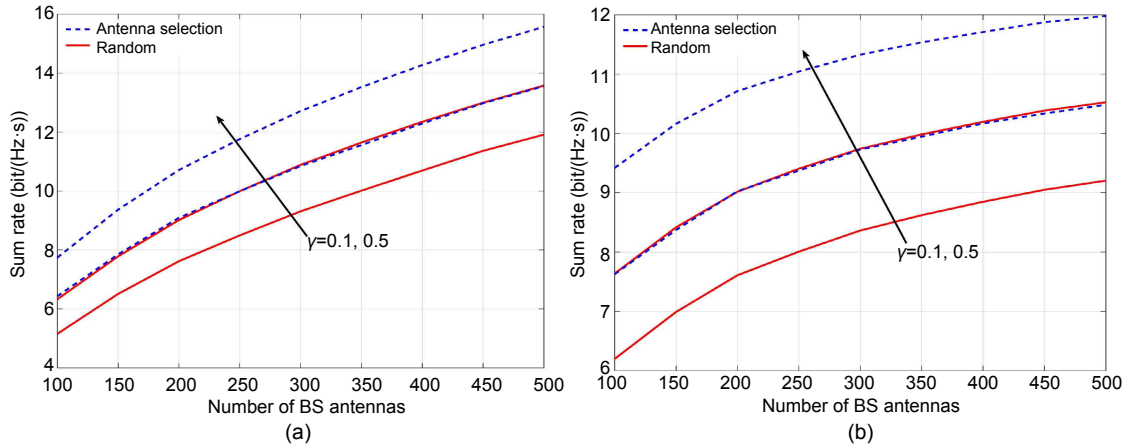

Fig. 4 Uplink sum rate of antenna selection and random connection against the number of BS antennas N_r for b=1 and γ=0.1, 0.5 with ρ=30 dB (a) and $\rho=E_u/N_{RF}$ with E_u=50 dB (b)

$\rho=E_u/N_{RF}$ with E_u=50 dB, respectively. It is observed that the sum rate at which the antenna selection algorithm is applied at γ=0.1 is approximately the same as the rate of random connection at γ=0.5. This shows that applying the antenna selection algorithm can greatly reduce the number of high-resolution ADCs to maintain a desirable rate. On the other hand, for ρ=30 dB, the sum rate increases to infinity when $N_r\to\infty$ but for $\rho=E_u/N_{RF}$, the sum rate reaches a constant. This proves the correctness of Remarks 3 and 4.

Fig. 5 presents the sum rate over the high-resolution ADC ratio γ with the number of antennas N_r=256 and transmit power ρ=30 dB for the number of quantization bits b=1, 2, ∞. The sum rate increases with the increase in the high-resolution ratio γ, and eventually increases to the rate of the full-resolution case, which is consistent with the actual situation. Compared to the approximate linear growth of random antenna selection, the antenna selection algorithm makes the sum rate increase faster with the increase of γ, and the rate at γ=0.7 is almost the same as the rate at full resolution. This indicates that we can make γ=0.7 to reduce the cost and power consumption of the system and apply the antenna selection algorithm to maintain the performance of the full-resolution system.

To explore the impact of analog-digital hybrid beamforming on system performance, Fig. 6 illustrates the sum rate over the ratio of the RF chain μ with the number of antennas N_r=256, transmit power ρ=30 dB, and high-resolution ADC ratio γ=0.5 for the number of quantization bits b=1, 2. Under the case of random connection, the difference in the system performance caused by quantization bits does not change as the ratio of the RF chain increases. However, as for the case of antenna selection connection, this difference continues to decrease and can be ignored when $\mu\geq$0.8. Therefore, when the ratio of the RF chain is large and antenna selection connection is applied, we can reduce the resolution of ADCs without causing loss to the achievable rate of the system.

5.2 Power allocation

We verify the promoting use of Algorithm 1 on the system sum rate in Fig. 7 with the total power P_T=40 dB. The uniform power allocation is the initialization in Algorithm 1, i.e., $\rho_k=P_T/(2N_u)$ and $P_B=P_T/2$. We can see that the power allocation algorithm clearly promotes the sum achievable rate compared with the uniform power allocation. For

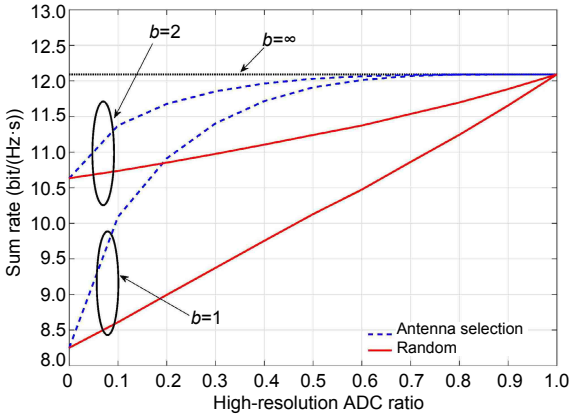

Fig. 5 Uplink sum rate of antenna selection and random connection against the high-resolution ADC ratio γ for N_r=256, ρ=30 dB, and b=1, 2, ∞

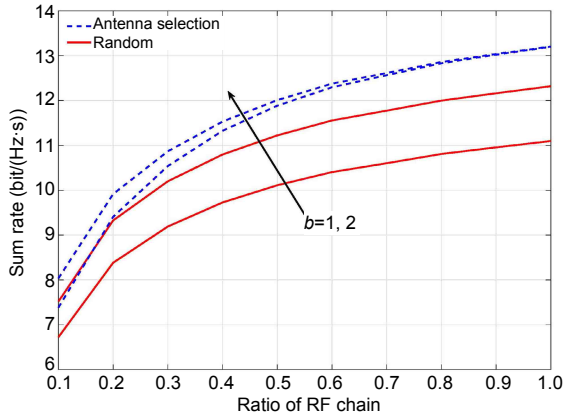

Fig. 6 Uplink sum rate of antenna selection and random connection against the ratio of the RF chain μ for γ=0.5, ρ=30 dB, and b=1, 2

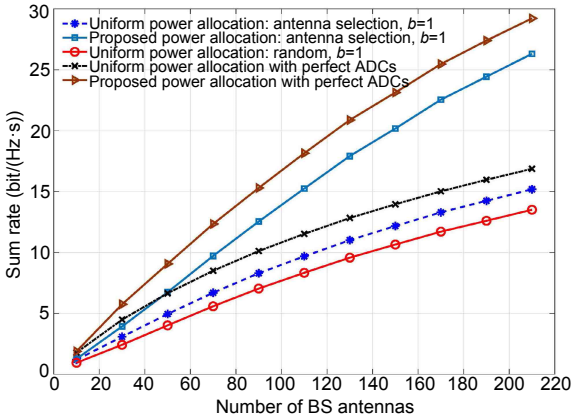

Fig. 7 Uplink sum rate of antenna selection and random connection against the number of antennas for P_T=40 dB

uniform power allocation with antenna selection, the power allocation algorithm improves the sum rate by about 50%, and for random connection, the improvement is about 70%. This confirms that power allocation is necessary in mixed-ADC multi-cell mmWave massive MIMO systems.

5.3 Energy efficiency

In this subsection, we investigate the EE of the mixed-ADC mmWave massive MIMO system to evaluate the tradeoff between SE and EE. EE can be defined as

$$\eta_{\mathrm{EE}} = B\frac{R_{\mathrm{sum}}}{P_{\mathrm{total}}}\ (\mathrm{bit/J}), \tag{40}$$

where B=1 GHz is the bandwidth and P_{total} is the total power consumed by the BS. Considering the system model in Fig. 1, P_{total} can be expressed as

$$\begin{aligned} P_{\mathrm{total}} = {} & N_{\mathrm{r}}(P_{\mathrm{LNA}} + P_{\mathrm{S}} + N_{\mathrm{RF}}P_{\mathrm{PS}}) + N_{\mathrm{RF}}(P_{\mathrm{RF}} + P_{\mathrm{C}}) \\ & + 2N_{\mathrm{RF0}}P_{\mathrm{HADC}} + 2N_{\mathrm{RF1}}P_{\mathrm{LADC}} + P_{\mathrm{BB}}, \end{aligned} \tag{41}$$

where P_{LNA}, P_{S}, P_{PS}, P_{RF}, P_{C}, P_{BB}, P_{HADC}, and P_{LADC} represent the power consumed by the low-noise amplifier (LNA), splitter, phase shifter (PS), RF chain, combiner, baseband processor, high-resolution ADCs, and low-resolution ADCs, respectively.

The power consumption parameters in the simulation are configured as P_{LNA}=39 mW, P_{S}=19.5 mW, P_{PS}=2 mW, P_{RF}=40 mW, P_{C}=19.5 mW, P_{BB}=200 mW (Abbas et al., 2017). Power consumed by ADC can be expressed as

$$P_{\mathrm{ADC}} = mB2^{b}, \tag{42}$$

where m is the ADC Walden figure and m=5–15 fJ per conversion step (Abbas et al., 2017) when B=1 GHz, and b is the number of quantization bits of ADC.

With the help of the power consumption models in Eqs. (41) and (42), EE of the multi-cell mmWave massive MIMO system with mixed-ADCs is studied in Figs. 8–10. We illustrate EE over the quantization bits with transmit power ρ=30 dB for N_{RF0}=0, 5, 10, 128 in Fig. 8. Systems with full low-resolution ADCs achieve the highest EE, which means that high-resolution ADCs reduce the EE. However, SE of the full-resolution ADC system is quite low and brings great difficulties to the front-end design of the system. Moreover, we can see in Fig. 8 that EE tends to rise first and then decrease, and peaks when b=3.

Fig. 9 demonstrates the power consumption of the receiver versus the uplink sum rate for different numbers of quantization bits. When the number of quantization bits is small, i.e., $b\leq$4, the sum rate of the system increases rapidly with the increase of the number of the quantization bits and the power consumption is almost constant. However, when b>4, the power consumption increases dramatically. The reason for this phenomenon is that the power consumption of ADCs is exponentially increasing. Thus, 4-bit ADCs will achieve the optimal tradeoff between the sum rate and power consumption.

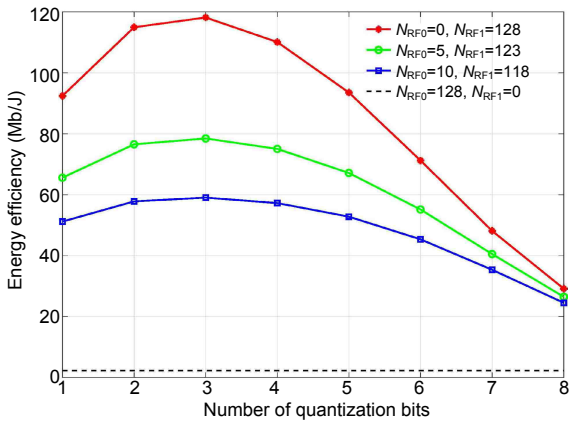

Fig. 8 Energy efficiency of multi-cell mixed-ADC mmWave massive MIMO systems over different numbers of ADC quantization bits with N_{r}=256 and N_{RF0}=0, 5, 10, 128

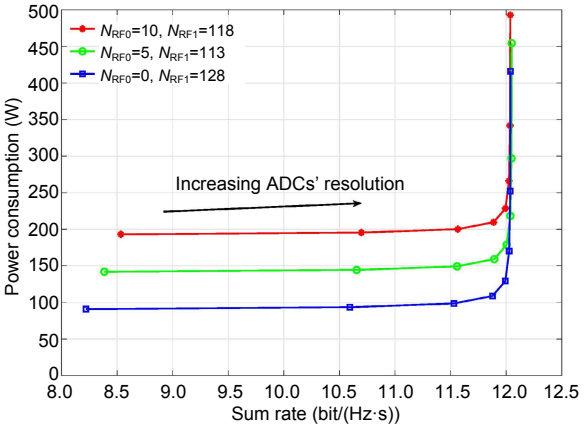

Fig. 9 Power consumption versus sum rate with N_{r}=256 and N_{RF0}=0, 5, 10

Fig. 10 depicts the effect of analog-digital hybrid beamforming on the EE. Comparing Fig. 6 with Fig. 10, we can see that the hybrid beamforming technology exchanges SE for EE. At the same time, the hybrid beamforming technology is more effective in improving EE when the high-precision ADC ratio is relatively low. In actual deployment, we can balance SE and EE to design the system architectural parameters.

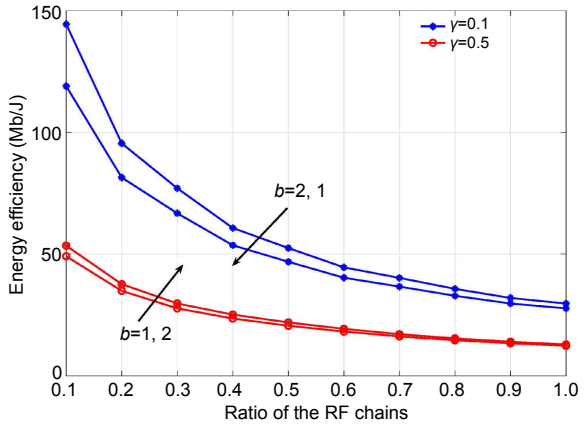

Fig. 10 Energy efficiency against RF chain ratio μ for b=1, 2

6 Conclusions

In this paper, we have investigated the achievable rate of a multi-cell mmWave massive MIMO system with a mixed-ADC and hybrid beamforming architecture considering antenna selection. Both exact and approximate closed-form expressions for the uplink achievable rate have been derived. Then, we have analyzed the impacts of the user transmit power, number of RF chains at BS, ratio of high-resolution ADCs, number of propagation paths, and number of quantization bits on the achievable rate, and proved that the user transmit power can be scaled down by $1/N_r$ to maintain a desirable rate. Numerical results have shown that employing the antenna selection algorithm is an effective method for improving the performance of the mixed-ADC system. We have proposed an efficient power allocation scheme which can significantly increase the sum achievable rate. Finally, we have investigated the EE and found that the system will achieve the highest EE and the best tradeoff between the achievable rate and power consumption when BS configures 3- and 4-bit ADCs, respectively.

Contributors

Tao ZHOU and Jiayi ZHANG designed the research. Tao ZHOU and Guichao CHEN drafted the manuscript. Cheng-xiang WANG, Liu LIU, and Yiqun LIANG helped organize the manuscript. Tao ZHOU and Jiayi ZHANG revised and finalized the paper.

Compliance with ethics guidelines

Tao ZHOU, Guichao CHEN, Cheng-xiang WANG, Jiayi ZHANG, Liu LIU, and Yiqun LIANG declare that they have no conflict of interest.

References

Abbas WB, Gomez-Cuba F, Zorzi M, 2017. Millimeter wave receiver efficiency: a comprehensive comparison of beamforming schemes with low resolution ADCs. *IEEE Trans Wirel Commun*, 16(12):8131-8146. https://doi.org/10.1109/TWC.2017.2757919

Akdeniz MR, Liu YP, Samimi MK, et al., 2014. Millimeter wave channel modeling and cellular capacity evaluation. *IEEE J Sel Area Commun*, 32(6):1164-1179. https://doi.org/10.1109/JSAC.2014.2328154

Ayach OE, Heath RW, Abu-Surra S, et al., 2012. Low complexity precoding for large millimeter wave MIMO systems. IEEE Int Conf on Communications, p.3724-3729. https://doi.org/10.1109/ICC.2012.6363634

Boccardi F, Heath RW, Lozano A, et al., 2014. Five disruptive technology directions for 5G. *IEEE Commun Mag*, 52(2): 74-80. https://doi.org/10.1109/MCOM.2014.6736746

Busari SA, Huq KMS, Mumtaz S, et al., 2018. Millimeter-wave massive MIMO communication for future wireless systems: a survey. *IEEE Commun Surv Tut*, 20(2):836-869. https://doi.org/10.1109/COMST.2017.2787460

Choi J, Evans BL, Gatherer A, 2017. Resolution-adaptive hybrid MIMO architectures for millimeter wave communications. *IEEE Trans Signal Process*, 65(23):6201-6216. https://doi.org/10.1109/TSP.2017.2745440

Choi J, Sung J, Evans BL, et al., 2018. Antenna selection for large-scale MIMO systems with low-resolution ADCs. IEEE Int Conf on Acoustics, Speech and Signal Processing, p.3594-3598. https://doi.org/10.1109/ICASSP.2018.8462107

Dai JX, Liu J, Wang JZ, et al., 2020. Asymptotic analysis of full-duplex large-scale MIMO systems with low-resolution ADCs/DACs over Rician fading channels. *IEEE Syst J*, 14(4):4832-4841. https://doi.org/10.1109/JSYST.2020.2966370

Heath RW, González-Prelcic N, Rangan S, et al., 2016. An overview of signal processing techniques for millimeter wave MIMO systems. *IEEE J Sel Top Signal Process*, 10(3):436-453. https://doi.org/10.1109/JSTSP.2016.2523924

Huang J, Wang CX, Feng R, et al., 2017. Multi-frequency mmWave massive MIMO channel measurements and characterization for 5G wireless communication systems. *IEEE J Sel Areas Commun*, 35(7):1591-1605. https://doi.org/10.1109/JSAC.2017.2699381

Huang J, Wang CX, Liu Y, et al., 2018. A novel 3D GBSM for mmWave MIMO channels. *Sci China Inform Sci*, 61(10): 102305. https://doi.org/10.1007/s11432-018-9480-4

Li YZ, Tao C, Seco-Granados G, et al., 2017. Channel estimation and performance analysis of one-bit massive MIMO systems. *IEEE Trans Signal Process*, 65(15): 4075-4089. https://doi.org/10.1109/TSP.2017.2706179

Liang N, Zhang WY, 2016. Mixed-ADC massive MIMO. *IEEE J Sel Areas Commun*, 34(4):983-997. https://doi.org/10.1109/JSAC.2016.2544604

Liu Y, Wang CX, Huang J, et al., 2019. Novel 3-D nonstationary mmWave massive MIMO channel models for 5G high-speed train wireless communications. *IEEE Trans Veh Technol*, 68(3):2077-2086. https://doi.org/10.1109/TVT.2018.2866414

Mollén C, Choi J, Larsson EG, et al., 2017. Uplink performance of wideband massive MIMO with one-bit ADCs. *IEEE Trans Wirel Commun*, 16(1):87-100. https://doi.org/10.1109/TWC.2016.2619343

Orhan O, Erkip E, Rangan S, 2015. Low power analog-to-digital conversion in millimeter wave systems: impact of resolution and bandwidth on performance. Information Theory and Applications Workshop, p.191-198. https://doi.org/10.1109/ITA.2015.7308988

Qiao D, Tan WQ, Zhao YY, et al., 2016. Spectral efficiency for massive MIMO zero-forcing receiver with low-resolution ADC. 8th Int Conf on Wireless Communications & Signal Processing, p.1-6. https://doi.org/10.1109/WCSP.2016.7752527

Rahimian S, Jing YD, Ardakani M, 2020. Performance analysis of massive MIMO multi-way relay networks with low-resolution ADCs. *IEEE Trans Wirel Commun*, 19(9): 5794-5806. https://doi.org/10.1109/TWC.2020.2997290

Tan WQ, Jin S, Wen CK, et al., 2016. Spectral efficiency of mixed-ADC receivers for massive MIMO systems. *IEEE Access*, 4:7841-7846. https://doi.org/10.1109/ACCESS.2016.2602798

Venkateswaran V, van der Veen A J, 2010. Analog beamforming in MIMO communications with phase shift networks and online channel estimation. *IEEE Trans Signal Process*, 58(8):4131-4143. https://doi.org/10.1109/TSP.2010.2048321

Wang CX, Haider F, Gao XQ, et al., 2014. Cellular architecture and key technologies for 5G wireless communication networks. *IEEE Commun Mag*, 52(2):122-130. https://doi.org/10.1109/MCOM.2014.6736752

Xu JD, Xu W, Zhang H, et al., 2019. Performance analysis of multi-cell millimeter-wave massive MIMO networks with low-precision ADCs. *IEEE Trans Commun*, 67(1):302-317. https://doi.org/10.1109/TCOMM.2018.2874963

You XH, Wang CX, Huang J, et al., 2021. Towards 6G wireless communication networks: vision, enabling technologies, and new paradigm shifts. *Sci China Inform Sci*, 64(1):110301. https://doi.org/10.1007/s11432-020-2955-6

Yu XH, Shen JC, Zhang J, et al., 2016. Alternating minimization algorithms for hybrid precoding in millimeter wave MIMO systems. *IEEE J Sel Top Signal Process*, 10(3): 485-500. https://doi.org/10.1109/JSTSP.2016.2523903

Zhang JY, Dai LL, He ZY, et al., 2017. Performance analysis of mixed-ADC massive MIMO systems over Rician fading channels. *IEEE J Sel Areas Commun*, 35(6):1327-1338. https://doi.org/10.1109/JSAC.2017.2687278

Zhang JY, Dai LL, He ZY, et al., 2019. Mixed-ADC/DAC multipair massive MIMO relaying systems: performance analysis and power optimization. *IEEE Trans Commun*, 67(1):140-153. https://doi.org/10.1109/TCOMM.2018.2869596

Zhang MJ, Tan WQ, Gao JH, et al., 2018. Spectral efficiency and power allocation for mixed-ADC massive MIMO system. *China Commun*, 15(3):112-127. https://doi.org/10.1109/CC.2018.8331995

Zhang Q, Jin S, Wong KK, et al., 2014. Power scaling of uplink massive MIMO systems with arbitrary-rank channel means. *IEEE J Sel Top Signal Process*, 8(5):966-981. https://doi.org/10.1109/JSTSP.2014.2324534

Zhang Y, Cheng YL, Zhou M, et al., 2020. Analysis of uplink cell-free massive MIMO system with mixed-ADC/DAC receiver. *IEEE Syst J*, in press. https://doi.org/10.1109/JSYST.2020.2999521

Zhou T, Tao C, Salous S, et al., 2018. Measurements and analysis of angular characteristics and spatial correlation for high-speed railway channels. *IEEE Trans Intell Transp Syst*, 19(2):357-367. https://doi.org/10.1109/TITS.2017.2681112

Zhou T, Yang Y, Liu L, et al., 2020a. A dynamic 3-D wideband GBSM for cooperative massive MIMO channels in intelligent high-speed railway communication systems. *IEEE Tran Wirel Commun*, in press. https://doi.org/10.1109/TWC.2020.3040392

Zhou T, Tao C, Salous S, et al., 2020b. Geometry-based multilink channel modeling for high-speed train communication networks. *IEEE Trans Intell Transp Syst*, 21(3): 1229-1238. https://doi.org/10.1109/TITS.2019.2905036

Appendix: Proof of Theorem 1

Applying Lemma 1 in Zhang Q et al. (2014), we can obtain the approximate solution of Eq. (14):

$$R_k = \log_2\left(1+\frac{\mathbb{E}\{D_k\}}{\mathbb{E}\{J_k\}}\right). \tag{A1}$$

For the MRC receive algorithm, the digital

receive matrix $\boldsymbol{A}$ in Eq. (11) can be expressed as

$$\boldsymbol{A}=\begin{bmatrix}\boldsymbol{A}_0\\ \boldsymbol{A}_1\end{bmatrix}=\begin{bmatrix}\boldsymbol{H}_0\\ \boldsymbol{H}_1\end{bmatrix}. \tag{A2}$$

The desired signal power in Eq. (15) can be expressed as

$$D_k=\rho\left(\left\|\boldsymbol{h}_{k,0}\right\|^4+\alpha^2\left\|\boldsymbol{h}_{k,1}\right\|^4+2\alpha\left|\left\|\boldsymbol{h}_{k,0}\right\|^2\left\|\boldsymbol{h}_{k,1}\right\|^2\right), \tag{A3}$$

and the interference-plus-noise power in Eq. (16) can be expressed as

$$\begin{aligned}J_k=&\rho\sum_{j=1,j\neq k}^{N_\mathrm{u}}\left|\boldsymbol{h}_{k,0}^\mathrm{H}\boldsymbol{h}_{j,0}\right|^2+\alpha^2\rho\sum_{j=1,j\neq k}^{N_\mathrm{u}}\left|\boldsymbol{h}_{k,1}^\mathrm{H}\boldsymbol{h}_{j,1}\right|^2\\&+\rho\sum_{n=1}^{N}\sum_{j=1}^{N_\mathrm{u}}\left|\boldsymbol{h}_{k,0}^\mathrm{H}\boldsymbol{h}_{n,j,0}\right|^2+\alpha^2\rho\sum_{n=1}^{N}\sum_{j=1}^{N_\mathrm{u}}\left|\boldsymbol{h}_{k,1}^\mathrm{H}\boldsymbol{h}_{n,j,1}\right|^2\\&+\left\|\boldsymbol{h}_{k,0}\right\|^2+\alpha^2\left\|\boldsymbol{h}_{k,1}\right\|^2+\boldsymbol{h}_{k,1}^\mathrm{H}\boldsymbol{R}_{\boldsymbol{n}_\mathrm{q}}\boldsymbol{h}_{k,1}.\end{aligned} \tag{A4}$$

We first define an indicator function f to characterize the sparsity of the channel matrix:

$$f_{\{i\in\Omega\}}=\begin{cases}1, & \text{if } i\in\Omega,\\ 0, & \text{otherwise.}\end{cases} \tag{A5}$$

With this indicator function f, the channel gain between the k^{th} user and the i^{th} RF chain can be expressed as

$$h_{k,i}=f_{\{i\in\Re_k\}}\sqrt{\beta_k}\,g_{k,i}c_{k,i},\ k=1,2,\cdots,N_\mathrm{u}, \tag{A6}$$

where $\Re_k=\{i|h_{k,i}\neq0,\ i=1,2,\ldots,N_\mathrm{RF}\}$.

We then calculate the expectation for the number of propagation paths L in Eq. (2):

$$\mathbb{E}\{L\}=\Pr(L=0)+\sum_{l=1}^{\infty}l\Pr(L=l)=\mathrm{e}^{-\lambda_\mathrm{p}}+\lambda_\mathrm{p}. \tag{A7}$$

Similarly, the expectation of L^2 can be derived as

$$\mathbb{E}\{L^2\}=P(L=0)+\sum_{l=1}^{\infty}l^2P(L=l)=\mathrm{e}^{-\lambda_\mathrm{p}}+\lambda_\mathrm{p}+\lambda_\mathrm{p}^2. \tag{A8}$$

We finally solve Eqs. (A3) and (A4) to obtain the result. For Eq. (A3), we first obtain

$$\begin{aligned}&\mathbb{E}\left\{\left\|\boldsymbol{h}_{k,0}\right\|^2\middle|L_k\right\}\\&=\sum_{i=1}^{N_\mathrm{RF0}}\mathbb{E}\left\{\left|h_{k,i}\right|^2\right\}\\&=\sum_{i=1}^{N_\mathrm{RF0}}\mathbb{E}\left\{\left|f_{\{i\in\Re_k\}}\sqrt{\beta_k}\,g_{k,i}c_{k,i}\right|^2\right\}\\&=\beta_k\overline{\left|c_{k,0}\right|^2}\left(\lambda_\mathrm{p}+\mathrm{e}^{-\lambda_\mathrm{p}}\right)\gamma.\end{aligned} \tag{A9}$$

Similarly, we can obtain

$$\mathbb{E}\left\{\left\|\boldsymbol{h}_{k,1}\right\|^2\middle|L_k\right\}=\beta_k\overline{\left|c_{k,1}\right|^2}\left(\lambda_\mathrm{p}+\mathrm{e}^{-\lambda_\mathrm{p}}\right)(1-\gamma). \tag{A10}$$

Then, we calculate $\mathbb{E}\left\{\left\|\boldsymbol{h}_{k,0}\right\|^4\middle|L_k\right\}$ as

$$\begin{aligned}&\mathbb{E}\left\{\left\|\boldsymbol{h}_{k,0}\right\|^4\middle|L_k\right\}\\&=\mathbb{E}\left\{\left(\sum_{i=1}^{N_\mathrm{RF0}}\left|h_{k,i}\right|^2\right)^2\right\}\\&=\mathbb{E}\left\{\left(\sum_{i=1}^{N_\mathrm{RF0}}\left|f_{\{i\in\Re_k\}}\sqrt{\beta_k}\,g_{k,i}c_{k,i}\right|^2\right)^2\right\}\\&=\beta_k^2\overline{\left|c_{k,0}\right|^4}\left(\lambda_\mathrm{p}+\mathrm{e}^{-\lambda_\mathrm{p}}\right)\gamma\\&\quad+\beta_k^2\left(\overline{\left|c_{k,0}\right|^2}\right)^2\left(\lambda_\mathrm{p}^2+\lambda_\mathrm{p}+\mathrm{e}^{-\lambda_\mathrm{p}}\right)\gamma^2.\end{aligned} \tag{A11}$$

Similarly, we can obtain

$$\begin{aligned}&\mathbb{E}\left\{\left\|\boldsymbol{h}_{k,1}\right\|^4\middle|L_k\right\}\\&=\beta_k^2\overline{\left|c_{k,1}\right|^4}\left(\lambda_\mathrm{p}+\mathrm{e}^{-\lambda_\mathrm{p}}\right)(1-\gamma)\\&\quad+\beta_k^2\left(\overline{\left|c_{k,1}\right|^2}\right)^2\left(\lambda_\mathrm{p}^2+\lambda_\mathrm{p}+\mathrm{e}^{-\lambda_\mathrm{p}}\right)(1-\gamma)^2.\end{aligned} \tag{A12}$$

Substituting Eqs. (A9)–(A12) into Eq. (A3), we can obtain the desired signal power as

$$
\begin{aligned}
&\frac{1}{\rho}\mathbb{E}\{D_k\}\\
&=\mathbb{E}\left\{\left(\left\|\boldsymbol{h}_{k,0}\right\|^2+\alpha\left\|\boldsymbol{h}_{k,1}\right\|^2\right)^2\right\}\\
&=\beta_k^2\left(\lambda_{\mathrm{p}}+\mathrm{e}^{-\lambda_{\mathrm{p}}}\right)\left[\overline{\left|c_{k,0}\right|^4}\gamma+\alpha^2\overline{\left|c_{k,1}\right|^4}(1-\gamma)\right]\\
&\quad+\beta_k^2\left(\lambda_{\mathrm{p}}^2+\lambda_{\mathrm{p}}+\mathrm{e}^{-\lambda_{\mathrm{p}}}\right)\left(\overline{\left|c_{k,0}\right|^2}\right)^2\gamma^2\\
&\quad+\alpha^2\beta_k^2\left(\lambda_{\mathrm{p}}^2+\lambda_{\mathrm{p}}+\mathrm{e}^{-\lambda_{\mathrm{p}}}\right)\left(\overline{\left|c_{k,1}\right|^2}\right)^2(1-\gamma)^2\\
&\quad+2\alpha\beta_k^2\left(\lambda_{\mathrm{p}}^2+\lambda_{\mathrm{p}}+\mathrm{e}^{-\lambda_{\mathrm{p}}}\right)\overline{\left|c_{k,0}\right|^2\left|c_{k,1}\right|^2}\gamma(1-\gamma).
\end{aligned}
\tag{A13}
$$

For Eq. (A4), we first calculate $\mathbb{E}\left\{\left|\boldsymbol{h}_{k,0}^{\mathrm{H}}\boldsymbol{h}_{j,0}\right|^2\middle|L_k\right\}$ as

$$
\begin{aligned}
&\mathbb{E}\left\{\left|\boldsymbol{h}_{k,0}^{\mathrm{H}}\boldsymbol{h}_{j,0}\right|^2\middle|L_k\right\}\\
&=\mathbb{E}\left\{\sum_{i=1}^{N_{\mathrm{RF0}}}h_{k,i}^*h_{j,i}\sum_{i=1}^{N_{\mathrm{RF0}}}h_{j,i}^*h_{k,i}\right\}\\
&=\sum_{i=1}^{N_{\mathrm{RF0}}}\mathbb{E}\left\{\left|h_{k,i}\right|^2\left|h_{j,i}\right|^2\right\}\\
&=\beta_k\beta_j\sum_{i=1}^{N_{\mathrm{RF0}}}\overline{\left|c_{k,0}\right|^2\left|c_{j,0}\right|^2}\mathbb{E}\left\{f_{\{i\in\Re_k,i\in\Re_j\}}\right\}\\
&=\beta_k\beta_j\overline{\left|c_{k,0}\right|^2\left|c_{j,0}\right|^2}\frac{1}{N_{\mathrm{RF}}}\left(\lambda_{\mathrm{p}}+\mathrm{e}^{-\lambda_{\mathrm{p}}}\right)^2\gamma.
\end{aligned}
\tag{A14}
$$

Similarly, we can obtain

$$
\begin{aligned}
&\mathbb{E}\left\{\left|\boldsymbol{h}_{k,1}^{\mathrm{H}}\boldsymbol{h}_{j,1}\right|^2\middle|L_k\right\}\\
&=\beta_k\beta_j\overline{\left|c_{k,1}\right|^2\left|c_{j,1}\right|^2}\frac{1}{N_{\mathrm{RF}}}\left(\lambda_{\mathrm{p}}+\mathrm{e}^{-\lambda_{\mathrm{p}}}\right)^2(1-\gamma),
\end{aligned}
\tag{A15}
$$

$$
\begin{aligned}
&\mathbb{E}\left\{\left|\boldsymbol{h}_{k,0}^{\mathrm{H}}\boldsymbol{h}_{n,j,1}\right|^2\middle|L_k\right\}\\
&=\beta_k\beta_{n,j}\overline{\left|c_{k,0}\right|^2\left|c_{n,j,0}\right|^2}\frac{1}{N_{\mathrm{RF}}}\left(\lambda_{\mathrm{p}}+\mathrm{e}^{-\lambda_{\mathrm{p}}}\right)^2\gamma.
\end{aligned}
\tag{A16}
$$

Then, using Eq. (10) we can obtain Eq. (A17) as

$$
\begin{aligned}
&\frac{1}{\alpha(1-\alpha)}\mathbb{E}\left\{\boldsymbol{h}_{k,1}^{\mathrm{H}}\boldsymbol{R}_{\boldsymbol{n}_q}\boldsymbol{h}_{k,1}\middle|L_k\right\}\\
&=\mathbb{E}\left\{\boldsymbol{h}_{k,1}^{\mathrm{H}}\mathrm{diag}\left(\rho\bar{\boldsymbol{H}}_1\bar{\boldsymbol{H}}_1^{\mathrm{H}}+\boldsymbol{I}_{N_{\mathrm{RF1}}}\right)\boldsymbol{h}_{k,1}\right\}\\
&=\mathbb{E}\left\{\sum_{i=1}^{N_{\mathrm{RF1}}}\left|h_{k,i}\right|^2\left(\rho\sum_{j=1}^{N_{\mathrm{u}}}\left|h_{j,i}\right|^2+\rho\sum_{n=1}^{N}\sum_{j=1}^{N_{\mathrm{u}}}\left|h_{n,j,i}\right|^2+1\right)\right\}\\
&=\beta_k\overline{\left|c_{k,1}\right|^2}\left(\lambda_{\mathrm{p}}+\mathrm{e}^{-\lambda_{\mathrm{p}}}\right)(1-\gamma)\\
&\quad+2\rho\beta_k^2\overline{\left|c_{k,1}\right|^4}\left(\lambda_{\mathrm{p}}+\mathrm{e}^{-\lambda_{\mathrm{p}}}\right)(1-\gamma)\\
&\quad+\rho\beta_k\sum_{j\neq k}^{N_{\mathrm{u}}}\beta_j\overline{\left|c_{k,1}\right|^2\left|c_{j,1}\right|^2}\frac{1}{N_{\mathrm{RF}}}\left(\lambda_{\mathrm{p}}+\mathrm{e}^{-\lambda_{\mathrm{p}}}\right)^2(1-\gamma)\\
&\quad+\rho\beta_k\sum_{n=1}^{N}\sum_{j=1}^{N_{\mathrm{u}}}\beta_{n,j}\overline{\left|c_{k,1}\right|^2\left|c_{n,j,1}\right|^2}\frac{1}{N_{\mathrm{RF}}}\left(\lambda_{\mathrm{p}}+\mathrm{e}^{-\lambda_{\mathrm{p}}}\right)^2(1-\gamma).
\end{aligned}
\tag{A17}
$$

Substituting Eqs. (A14)–(A17) into Eq. (A4), we obtain the interference-plus-noise power as

$$
\begin{aligned}
&\mathbb{E}\{J_k\}\\
&=\rho\beta_k\left(\mathrm{e}^{-\lambda_{\mathrm{p}}}+\lambda_{\mathrm{p}}\right)^2\\
&\quad\cdot\sum_{j\neq k}^{N_{\mathrm{u}}}\beta_j\frac{1}{N_{\mathrm{RF}}}\left[\overline{\left|c_{k,0}\right|^2\left|c_{j,0}\right|^2}\gamma+\alpha\overline{\left|c_{k,1}\right|^2\left|c_{j,1}\right|^2}(1-\gamma)\right]\\
&\quad+\rho\beta_k\left(\lambda_{\mathrm{p}}+\mathrm{e}^{-\lambda_{\mathrm{p}}}\right)^2\sum_{n=1}^{N}\sum_{j=1}^{N_{\mathrm{u}}}\beta_{n,j}\\
&\quad\cdot\frac{1}{N_{\mathrm{RF}}}\left[\overline{\left|c_{k,0}\right|^2\left|c_{n,j,0}\right|^2}\gamma+\overline{\left|c_{k,1}\right|^2\left|c_{n,j,1}\right|^2}(1-\gamma)\right]\\
&\quad+\beta_k\left(\lambda_{\mathrm{p}}+\mathrm{e}^{-\lambda_{\mathrm{p}}}\right)\left[\overline{\left|c_{k,0}\right|^2}\gamma+\alpha\overline{\left|c_{k,1}\right|^2}(1-\gamma)\right]\\
&\quad+2\alpha(1-\alpha)\rho\beta_k\left(\lambda_{\mathrm{p}}+\mathrm{e}^{-\lambda_{\mathrm{p}}}\right)\overline{\left|c_{k,1}\right|^4}(1-\gamma).
\end{aligned}
\tag{A18}
$$

Substituting Eqs. (A13) and (A18) into Eq. (A1), we obtain the final result in Eq. (17).